Electronic Structure of Metalloporphyrins. 1. Experimental Electron Density Distribution of (*meso*-Tetraphenylporphinato)cobalt(II)

Edwin D. Stevens

Contribution from the Department of Chemistry, State University of New York at Buffalo, Buffalo, New York 14214. *Received November 3, 1980. Revised Manuscript Received March 23, 1981*

Abstract: The electron density distribution of (*meso*-tetraphenylporphinato)cobalt(II), $C_{44}H_{28}N_4Co$, has been determined from high-resolution single-crystal X-ray diffraction measurements at 100 K. Intensities of 19909 reflections were collected by using Nb-filtered Mo Kα radiation to a resolution of $(\sin\theta)/\lambda = 1.20$ Å^{-1}. Averaging symmetry-related reflections yielded a set of 2409 independent reflections which refined by conventional least-squares techniques to $R = 3.4\%$ and $R_w = 3.8\%$. Maps of the deformation electron distribution have been calculated from the X-ray data by using parameters from refinement of high-order data ($(\sin\theta)/\lambda > 0.85$ Å^{-1}) and from model structure factors of a multipole deformation refinement. Improved estimates of the experimental phases afforded by the multipole refinement yield significant improvement in the electron density maps. The splitting of the cobalt d orbitals by the ligand field is clearly revealed in the observed density by eight peaks of 1.1 (1) e Å^{-3} at 0.45 Å from the cobalt directed into the faces of a coordination octahedron consisting of the porphyrin nitrogen atoms and the two unoccupied axial positions. Apparent orbital occupancies of 3.7 (3), 1.3 (2), 1.0 (2), and 1.0 (2) for the e, b_2, a_1, and b_1 orbitals on cobalt, respectively, are obtained from the refined X-ray multipole populations. Examination of the electron distribution in the porphyrin ring suggests some localization of π character in the C2–C3 bond.

The electronic structure of hemoproteins and transition-metal porphyrin models has been of great interest for many years because of the apparent involvement of both electronic and stereochemical changes in the mode of biological action.[1] Of particular interest is the mechanism of cooperative binding of dioxygen in the oxygen-transport protein hemoglobin. X-ray structural studies of hemoproteins and a large number of metalloporphyrins, especially "picket-fence" porphyrins, have established the stereochemical details of the active site.[2] Several aspects of the electronic structure of the active site, however, remain to be resolved.

A large number of different physical probes have been applied in the study of metalloporphyrins.[3] Results are limited, however, since generally each probe provides information on only a single aspect of the molecular electron distribution. Metalloporphyrins are therefore an ideal class for the direct experimenttal determination of the electron density distribution by high-resolution X-ray diffraction measurements. Several studies have shown that charge density distributions may be determined with an accuracy comparable to the most sophisticated theoretical calculations on small molecules.[4] Also, recent results on structures containing transition metals have shown that d-electron configurations may be successfully determined from the experiment.[5,6]

By examination and analysis of the experimental electron distributions of a selected series of iron porphyrins at low temperature, several specific questions dealing with the electronic structure and its relationship to the cooperativity mechanism of dioxygen binding can be answered. The size of the iron atom and its change on going from high spin to low spin can be determined. The d-electron configuration of the iron atom may be determined in each combination of coordination number, spin state, and oxygen state. The distribution of partial charges among the iron, porphyrin, and coordinated ligand atoms may be obtained by integration of the experimental density. Finally, the nature of the bonding, including the relative contributions of σ and π bonding, may be determined for bonds between the iron and the ligands and between the iron and the porphyrin molecule.

Table I. Experimental Data

space group	$I\bar{4}2d$
temp, K	100 (5)
cell dimens	
a, Å	14.980 (4)
c, Å	13.704 (4)
X-ray wavelength Kα_1, Å	0.709 30
d(calcd), g/cm^3	1.451
abs coeff μ, cm^{-1}	5.95[a]
transmission factors, range	0.62–0.69
scan mode	θ:2θ step scans
step size	0.03° 2θ
scan width	2θ(Kα_1) − 1.2° to 2θ(Kα_2) + 1.2°
detector apeture	5 × 5 mm
crystal to detector distance	220 mm
take-off angle, deg	3.0

[a] Based on mass absorption coefficients from ref 13.

Due to the experimental difficulties such as poor crystal quality and disorder often encountered in crystal structure analysis of metalloporphyrins, the feasibility of accurate charge density studies on systems such as the iron porphyrins is uncertain. One room-temperature study at low resolution, however, has already appeared.[7] The present study of cobalt(II) *meso*-tetraphenylporphyrin (CoTPP) was undertaken to test the suitability of metalloporphyrins for charge density analysis. Further studies on iron porphyrins are in progress.

An additional benefit is that the experimental electron distribution can be used to calculate other one-electron properties of the molecule such as dipole moments, electrostatic potentials, and electric field gradients. The experimental density can therefore be used to correlate data obtained by other physical techniques. Until recently, molecules as large as metalloporphyrins were beyond the capabilities of reliable theoretical techniques.[8] As the theoretical methods are improved, the experimental electron distribution may be used as a critical test against which calcu-

(1) Perutz, M. F. *Br. Med. Bull.* **1976**, *32*, 195–208. Hoard, J. L. In "Porphyrins and Metalloporphyrins"; Smith, K. M. Ed.; Elsevier: Amsterdam, 1975; pp 317–380. Collman, J. P. *Acc. Chem. Res.* **1977**, *10*, 265–272.
(2) Collman, J. P.; Gagne, R. R.; Robinson, W. T.; Rodley, G. A. *Proc. Natl. Acad. Sci. U.S.A.* **1974**, *71*, 1326–1330. Jameson, G. B.; Molinaro, F. S.; Ibers, J. A.; Collman, J. P.; Brauman, J. I.; Rose, E.; Suslick, K. S. *J. Am. Chem. Soc.* **1980**, *102*, 3224–3237.
(3) See, for example: Volumes III, IV, and V of "The Porphyrins"; Dolphin, D., Ed.; Academic Press: New York, 1978.
(4) Stevens, E. D. *Acta Crystallogr., Sect. B* **1980**, *B36*, 1876–1886. Stevens, E. D.; Rys, J.; Coppens, P. *J. Am. Chem. Soc.* **1978**, *100*, 2324–2328. Stevens, E. D.; Rys, J.; Coppens, P. *Ibid.* **1977**, *99*, 265–267.
(5) Stevens, E. D.; DeLucia, M. L.; Coppens, P. *Inorg. Chem.* **1980**, *19*, 813–820.
(6) Iwata, M. *Acta Crystallogr., Sect. B* **1977**, *B33*, 59–69. Rees, B.; Mitschler, A. *J. Am. Chem. Soc.* **1976**, *98*, 7918–7924.
(7) Jameson, G. B.; Ibers, J. A. *J. Am. Chem. Soc.* **1978**, *18*, 1200–1208.
(8) Kirchner, R. F.; Loew, G. H. *J. Am. Chem. Soc.* **1977**, *99*, 4639–4647. Olafson, B. D.; Goddard, W. A. *Proc. Natl. Acad. Sci. U.S.A.* **1977**, *74* 1315–1319. Case, D. A.; Huynh, B. H.; Karplus, M. *J. Am. Chem. Soc.* **1979**, *101*, 4433–4453. Dedieu, A.; Rohmer, M.-M.; Veillard, H.; Veillard, A. *Nouv. J. Chim.* **1979**, *3*, 653–667.

0002-7863/81/1503-5087$01.25/0

Table II. Summary of Least-Squares Refinements

	refinement		
	I	II	III
(sin θ)/λ range, Å^{-1}	0.0–1.2	0.8–1.2	0.0–1.2
N_{obsd}	2308	591	2306
N_v	139	111	201
scale factor	0.5340 (8)	0.5113 (43)	0.5257 (7)
R factors,[a] %			
R	3.44	2.97	2.58
R_w	3.76	2.92	2.55
R factors including rejected reflections,[a] %			
R	3.88	3.73	2.70
R_w	3.78	3.96	2.57
GOF[b]	1.86	1.05	1.25

[a] $R = \Sigma||F_o| - k|F_c||/\Sigma|F_o|$; $R_w = (\Sigma w(|F_o| - k|F_c|)^2/(\Sigma w F_o^2))^{1/2}$. [b] "Goodness of fit" = GOF = $(\Sigma w(|F_o| - k|F_c|)^2/(N_{obsd} - N_v))^{1/2}$.

lations may be judged. A comparison of the experimental densitiy of CoTPP with a theoretical calculation will be reported later.[9]

Experimental Section

Sample Preparation and Data Collection. CoTPP was obtained from Strem Chemicals and crystallized in a Soxhlet extractor.[10] Large crystals were obtained by seeding the batch with the largest crystals of a preceding batch. A bipyramidal crystal with dimensions 0.46 × 0.46 × 0.35 mm was mounted on a Picker FACS-I automatic diffractometer, controlled by the Vanderbilt disk operating system,[11] and cooled to 100 ± 5 K with a stream of cold nitrogen gas generated with a locally modified Enraf-Nonius universial low-temperature device. During data collection, the gas-stream temperature was maintained within ±1 K as monitored with a copper–constantan thermocouple. Unit cell dimensions were obtained by least-squares refinement on the observed setting angles of the $K\alpha_1$ peaks of 30 centered reflections with $2\theta > 60°$. Scans of several systematically absent reflections and comparison of several symmetry-related relfections confirmed the space group as $I\bar{4}2d$. Crystal data for CoTPP are summarized in Table I.

X-ray intensity measurements were collected with Nb-filtered Mo Kα radiation by using a θ:2θ step scan technique. Each reflection was scanned from $2\theta(K\alpha_1) - 1.2°$ to $2\theta(K\alpha_2) + 1.2°$ by using a step size of 0.03° in 2θ and a count time of 1 s/step. The full-step scan profile of each reflection was recorded on magnetic tape and later analyzed to give the integrated intensity and estimated standard deviation.[12] An initial data set of 2412 reflections was collected in one octant with $(\sin\theta)/\lambda < 0.70$ Å^{-1}.

Since a large proprotion of the reflections at higher angles are weak, parameters from least-squares refinement of the preliminary data were used to predict the intensities of higher order reflections. Only reflections with intensities predicted to be greater than 5 times their estimated standard deviations were measured in the range $0.70 < (\sin\theta)/\lambda < 1.20$ Å^{-1}. For high angle reflections, the count time was increased to 2 s/step. Intensity measurements were made in four octants of reciprocal space having the same dispersion contribution,[13] yielding eight symmetry-related observations of each reflection. A total of 19909 measurements were collected, including 8400 with $(\sin\theta)/\lambda > 0.70$ Å^{-1}.

Seven standard reflections remeasured after every 100 reflections showed gradual fluctuations of ±2% during data collection. Corrections to the intensity measurements and contributions to the esd's were calculated from the behavior of the standards as described by McCandlish, Stout, and Andrews.[14]

Absorption corrections calculated by Gaussian numerical integration[15] were applied and symmetry-related observations averaged to give a final set of 2409 independent reflections. The internal agreement factors[16] for symmetry-related reflections were $R(F^2) = 6.8\%$ and $R_w(F^2) = 9.2\%$. The internal agreement is somewhat poorer than those commonly obtained in electron density studies of small molecules and may be due in part to the large number of weak reflections in the data set. For the 3405 strongest reflections ($F^2 > 100\sigma(F^2)$), the agreement factors were $R(F^2) = 3.8\%$ and $R_w(F^2) = 3.7\%$.

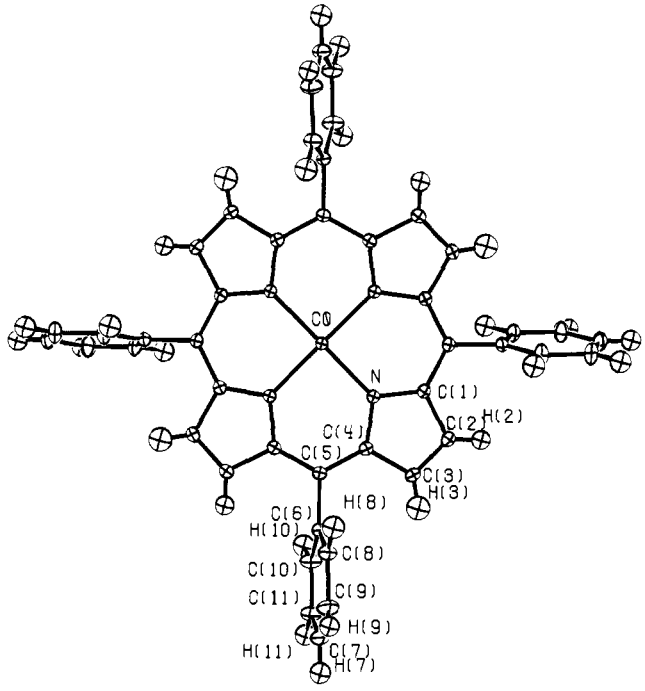

Figure 1. Plot of the CoTPP molecule viewed down the $\bar{4}$ axis. The label assigned to each crystallographically unique atom is displayed. Thermal ellipsoids are plotted at the 50% probability level.

Least-Squares Refinements. The quantity $\sum w(F_o/k - |F_c|)^2$ with $w = 1/\sigma^2(F_o)$ was minimized by full-matrix least-squares refinement. The estimated standard deviation of each observation, $\sigma(F_o^2)$ was taken as the larger of σ_1 and σ_2, where $\sigma_1^2 = \sigma_{count}^2 + \sigma_{scaling}^2 + (0.02F^2)^2$ and $\sigma_2^2 = \sum_i^N (F_{oi}^2 - \langle F_o^2\rangle)^2/(N-1)$ for N measurements of symmetry-related reflections. Reflections with both F_o and F_c less than $3\sigma(F)$ were considered "unobserved" and were not included in the refinement.

Core, valence, and total atomic scattering factos for Co, N, C, and H were taken from ref 13. Anomalous scattering factors for Co, N, and C from ref 17 were included in the calculation. Initial atomic coordinates for the refinement were taken from the room-temperature structure.[10] After several cycles, difference electron density maps were calculated, revealing the location of all hydrogen atoms. The hydrogens were then included in the least-squares refinement with isotropic thermal parameters and with use of a contracted hydrogen scattering factor.[18]

The occupancy of the cobalt was allowed to vary in an initial refinement to test for possible contamination of the sample with the free TPP base. Only data with $(\sin\theta)/\lambda > 0.80$ Å^{-1} were included to avoid bias from features of the valence density. Refinement yielded an occupancy for Co of 1.02 (5) which was judged sufficiently close to the ideal value. In all subsequent refinements the ideal stoichiometry was used.

Refinement converged at $R(F) = 5.83\%$ and $R_w(F) = 6.97\%$. After the signs of the reflection indices were changed, refinement converged at $R(F) = 3.44\%$ and $R_w(F) = 3.76\%$, indicating that the experimental measurements corresponded to the set $\{\bar{h}\bar{k}\bar{l}\}$ rather than the originally assigned set $\{hkl\}$. An ORTEP plot of CoTPP at 100 K giving the labeling scheme used for the crystallographically unique atoms is shown in Figure 1.

It is well-known that aspherical features of the valence electron distribution introduce a bias in positional and thermal parameters determined by X-ray diffraction.[19] This bias can be greatly reduced by including in the least-squares refinement only data collected at high angles where the scattering is primarily due to the core electrons.[20] Results of a high-order refinement on data with $(\sin\theta)/\lambda > 0.85$ Å^{-1} are given in Table III (refinement II). Since hydrogen contributes very little to scattering at high angles, bias-free hydrogen parameters cannot be determined from X-ray measurements except with data of unusually high

(9) Bénard, M.; Stevens, E. D., to be submitted for publication.
(10) Madura, P.; Scheidt, W. R. *Inorg. Chem.* **1976**, *15*, 3182–3185.
(11) Lenhert, P. G. *J. Appl. Crystallogr.* **1975**, *8*, 568–570.
(12) Blessing, R.; Coppens, P.; Becker, P. J. *J. Appl. Crystallogr.* **1974**, *7*, 488–492.
(13) "International Tables for X-ray Crystallography"; Kynoch Press: Birmingham, England, 1974; Vol. 4.
(14) McCandlish, L. E.; Stout, G. H.; Andrews, L. C. *Acta Crystallogr., Sect. A* **1975**, *A31*, 245–249.
(15) Coppens, P.; Leiserowitz, L.; Rabinovich, D. *Acta Crystallogr.* **1965**, *18*, 1035–1038.
(16) $R(F^2) = \sum_i|F_i^2 - \langle F_c^2\rangle|/\sum_i F_i^2$; $R_w(F^2) = (\sum_i w_i|F_i^2 - \langle F_i^2\rangle|^2/\sum_i w_i F_i^4)^{1/2}$; $w_i = 1/\sigma^2(F_i^2)$.
(17) Cromer, D. T.; Liberman, D. *J. Chem. Phys.* **1970**, *53*, 1891–1898.
(18) Stewart, R. F.; Davidson, E. R.; Simpson, W. T. *J. Chem. Phys.* **1965**, *42*, 3175–3187.
(19) Coppens, P *Acta Crystallogr., Sect. B* **1974**, *B30* 225–261.
(20) Stevens, E. D.; Hope, H. *Acta Crystallogr., Sect. A* **1975**, *A31*, 494–498.

Table III. Atomic Fractional Coordinates and Thermal Parameters ($\times 10^4$ Å^2)[a]

	x	y	z	U_{11}	U_{22}	U_{33}	U_{12}	U_{13}	U_{23}
Co	0.000 00	0.000 00	0.000 00	113 (1)	113	144 (1)	0	0	0
	0.000 00	0.000 00	0.000 00	105 (1)	105	135 (2)	0	0	0
	0.000 00	0.000 00	0.000 00	100 (1)	100	122 (1)	0	0	0
N	0.112 53 (7)	0.065 14 (7)	−0.001 79 (9)	117 (3)	127 (3)	177 (4)	0 (3)	−3 (4)	3 (4)
	0.112 51 (11)	0.065 82 (11)	−0.001 93 (22)	112 (4)	121 (4)	176 (6)	−11 (3)	−9 (6)	2 (6)
	0.112 45 (5)	0.065 34 (5)	−0.001 98 (6)	116 (2)	125 (2)	184 (3)	−1 (2)	−7 (3)	2 (3)
C1	0.196 68 (9)	0.032 87 (8)	0.018 24 (10)	125 (4)	148 (4)	193 (5)	−5 (4)	−13 (4)	−9 (4)
	0.196 58 (15)	0.032 59 (16)	0.018 01 (20)	117 (6)	137 (6)	177 (9)	−3 (5)	−14 (5)	0 (5)
	0.196 43 (6)	0.032 63 (6)	0.018 12 (7)	123 (3)	133 (3)	213 (3)	1 (4)	−15 (3)	−1 (3)
C2	0.261 15 (9)	0.103 51 (10)	0.017 21 (11)	137 (5)	172 (5)	302 (6)	−17 (4)	−30 (4)	2 (5)
	0.261 24 (18)	0.103 64 (20)	0.017 23 (33)	124 (6)	149 (6)	331 (16)	−18 (5)	−26 (7)	22 (7)
	0.261 50 (7)	0.103 52 (7)	0.017 19 (8)	134 (3)	159 (3)	326 (5)	−14 (3)	−27 (3)	9 (3)
C3	0.217 06 (9)	0.179 22 (9)	−0.007 20 (12)	151 (4)	150 (4)	300 (6)	−31 (4)	−6 (5)	16 (5)
	0.216 85 (16)	0.179 06 (17)	−0.007 01 (34)	226 (6)	146 (6)	323 (15)	−26 (5)	−10 (8)	36 (8)
	0.216 99 (6)	0.179 52 (7)	−0.007 34 (8)	136 (3)	147 (3)	313 (4)	−25 (3)	−16 (3)	21 (4)
C4	0.124 23 (9)	0.155 58 (9)	−0.017 35 (9)	143 (4)	137 (4)	191 (5)	−11 (4)	−9 (4)	1 (4)
	0.124 02 (16)	0.155 29 (15)	−0.017 02 (21)	132 (6)	122 (6)	184 (8)	−12 (4)	−13 (5)	7 (5)
	0.124 39 (6)	0.155 43 (6)	−0.017 44 (6)	133 (3)	124 (3)	211 (4)	−3 (3)	−13 (3)	10 (3)
C5	0.056 98 (9)	0.217 78 (9)	−0.031 50 (10)	150 (5)	126 (4)	171 (4)	−1 (4)	1 (4)	12 (4)
	0.057 21 (18)	0.217 73 (15)	−0.031 61 (22)	144 (6)	122 (5)	184 (9)	−4 (5)	−2 (6)	20 (5)
	0.056 79 (6)	0.217 85 (7)	−0.031 46 (7)	141 (4)	124 (3)	193 (4)	−3 (3)	−4 (3)	14 (3)
C6	0.082 06 (9)	0.311 14 (9)	−0.056 63 (10)	147 (4)	126 (4)	190 (5)	−11 (4)	−14 (4)	−11 (4)
	0.082 10 (7)	0.311 01 (15)	−0.056 62 (2)	154 (6)	113 (5)	179 (8)	−10 (5)	−7 (6)	6 (5)
	0.082 13 (6)	0.311 08 (6)	−0.056 80 (7)	159 (3)	125 (3)	178 (3)	−13 (3)	−10 (3)	7 (3)
C7	0.132 69 (11)	0.484 80 (10)	−0.106 11 (11)	254 (6)	160 (6)	280 (6)	−38 (5)	−3 (5)	36 (4)
	0.132 75 (25)	0.485 27 (19)	−0.106 02 (36)	251 (10)	128 (7)	257 (16)	−37 (5)	−3 (9)	30 (6)
	0.132 74 (8)	0.484 97 (6)	−0.106 09 (7)	261 (4)	143 (4)	264 (4)	−39 (3)	0 (3)	31 (3)
C8	0.105 04 (11)	0.332 41 (10)	−0.152 44 (10)	246 (6)	155 (5)	199 (5)	−19 (5)	19 (5)	10 (4)
	0.105 19 (23)	0.332 49 (17)	−0.152 75 (27)	253 (9)	138 (6)	179 (8)	−22 (6)	19 (7)	9 (6)
	0.104 85 (8)	0.332 52 (7)	−0.152 56 (7)	253 (3)	191 (3)	191 (3)	−24 (3)	23 (3)	9 (3)
C9	0.130 10 (13)	0.418 82 (11)	−0.177 15 (12)	327 (8)	188 (6)	231 (6)	−47 (6)	45 (6)	37 (5)
	0.129 92 (33)	0.418 95 (22)	−0.177 34 (33)	352 (15)	160 (7)	212 (11)	−40 (9)	49 (10)	30 (8)
	0.130 07 (9)	0.418 96 (8)	−0.177 26 (8)	338 (5)	176 (4)	222 (4)	−51 (4)	42 (4)	32 (3)
C10	0.084 62 (13)	0.377 91 (10)	0.013 67 (11)	343 (8)	158 (5)	204 (6)	−51 (6)	2 (5)	−3 (4)
	0.083 92 (34)	0.377 98 (20)	0.014 23 (24)	352 (14)	144 (7)	174 (10)	−57 (8)	−7 (9)	−9 (6)
	0.084 55 (9)	0.377 86 (7)	0.013 93 (7)	354 (5)	152 (3)	189 (4)	−53 (4)	8 (4)	−6 (3)
C11	0.109 84 (12)	0.464 45 (10)	−0.010 52 (12)	324 (7)	148 (5)	263 (6)	−42 (5)	−13 (6)	−10 (5)
	0.109 38 (32)	0.464 34 (21)	−0.010 63 (35)	338 (12)	132 (6)	236 (14)	−43 (7)	−18 (10)	−5 (7)
	0.110 03 (8)	0.464 41 (7)	−0.010 57 (8)	336 (5)	145 (3)	241 (4)	−49 (4)	−10 (4)	−10 (3)

	x	y	z	U,[b] Å^2		x	y	z	U,[b] Å^2
H2	0.318 92 (18)	0.090 02 (17)	0.027 10 (17)	262 (61)	H9	0.139 42 (17)	0.438 06 (16)	−0.238 46 (17)	254 (56)
	0.331 20	0.087 16	0.029 21	262		0.141 39	0.442 14	−0.251 47	254
	0.331 20	0.087 16	0.029 21	262		0.141 39	0.442 14	−0.251 47	254
H3	0.241 79 (21)	0.233 37 (20)	−0.008 83 (30)	406 (72)	H10	0.065 50 (10)	0.363 98 (19)	0.080 34 (19)	349 (69)
	0.247 29	0.245 39	−0.009 18	406		0.063 35	0.362 42	0.087 83	349
	0.247 29	0.245 39	−0.009 18	406		0.063 35	0.362 42	0.087 83	349
H7	0.149 82 (18)	0.540 53 (15)	−0.121 65 (20)	303 (65)	H11	0.111 27 (17)	0.512 10 (21)	0.035 07 (15)	321 (63)
	0.153 46	0.552 38	−0.124 95	303		0.111 49	0.519 18	0.041 85	321
	0.153 46	0.552 38	−0.124 95	303		0.111 49	0.519 18	0.041 85	321
H8	0.102 37 (19)	0.282 13 (19)	−0.196 90 (17)	334 (67)					
	0.102 04	0.275 89	−0.202 42	334					
	0.102 04	0.275 89	−0.202 42	334					

[a] First line, refinement I; second line, refinement II, third line, refinement III. [b] Isotropic temperature factors for hydrogen atoms ($U_{iso} = B_{iso}/(8\pi^2)$).

quality.[21] For CoTPP, approximate hydrogen positions have been determined by extending each hydrogen along the C–H bond vector, as determined in refinement I, to a distance of 1.09 Å from the carbon atom.

An alternative technique for avoiding bias in the refined parameters is to include additional variables in the least-squares refinement which describe the aspherical features of the valence density.[22,23] In the model used here, deformations of the electron density at each atom are described by an expansion of multipole density functions

$$\rho(\mathbf{r}) = \sum_{\text{atoms}} [\rho_{\text{core}}(\mathbf{r}) + P_v \rho_{\text{valence}}(\kappa r) + \sum_{l=0}^{4} R_l(\kappa' r) \sum_{m=-l}^{l} P_{lm} y_{lm}(\mathbf{r}/r)]$$

where ρ_{core} and ρ_{valence} are spherical Hartree–Fock core and valence densities and the y_{lm} are spherical harmonic angular functions in real form. The radial functions $R_{lm}(r)$ are given by

$$R_{lm} = Nr^n \exp(-\zeta r)$$

where N is a normalization factor and n and ζ are chosen for each l as described previously.[5,23] The P_v, P_{lm}, κ, and κ' are refinable parameters. Positional and thermal parameters for the hydrogens have been fixed in the same manner as in the high-order refinement (refinement II). Positional and thermal parameters from the multipole deformation refinement are listed in Table III (refinement III) and multipole populations in Table IV.

Electron Density Maps. Distortions of the atomic electron distribution as a result of chemical bonding in a molecule are best revealed in a plot of the deformation density, $\Delta\rho = \rho_{\text{obsd}}/\text{k} - \sum\rho_{\text{spherical atoms}}$, given by the difference between the total observed density and the density calculated for a superposition of spherical, neutral atoms (the "promolecule"). *Observed* deformation maps, $\Delta\rho(X - X_{\text{HO}})$, have been calculated by using the full X-ray data set to a resolution $(\sin\theta)/\lambda = 1.20$ Å^{-1} and corrected for anomalous dispersion. Positions and thermal parameters used in calculating the promolecule density have been taken from the high-order

(21) Hope, H. *Am. Crystallogr. Assoc. Prog. Abstr., Ser. 2*, **1980**, *7*, 35. Stevens, E. D. *Acta Crystallogr., Sect B* **1978**, *B34*, 544–551.

(22) Dawson, B. *Proc. R. Soc. London, Sect. A.* **1967**, *298*, 255–288. Harel, M.; Hirshfield, F. L. *Acta Crystallogr., Sect. B* **1975**, *B31* 162–172. Stewart, R. F. *Acta Crystallogr., Sect. A* **1976**, *A32*, 565–574.

(23) Hansen, N. K.; Coppens, P. *Acta Crystallogr., Sect. A* **1978**, *A34*, 909–921.

Table IV. Multipole Populations and Radial Exponents[a-c]

	Co	N	C(1)	C(2)	C(5)	C(6)	C(7)
κ	1.00	0.97 (1)	1.03 (1)	1.01 (1)	1.04 (1)	0.98 (1)	1.00 (1)
$\kappa'\zeta$	7.61 (3)	2.16 (7)	3.82 (16)	2.95 (10)	4.34 (36)	2.53 (9)	2.62 (5)
P_V	0.00	5.77 (9)	3.98 (13)	4.26 (11)	4.00 (15)	4.52 (11)	3.91 (6)
P_{00}	7.00	0.00	0.00	0.00	0.00	0.00	0.00
P_{11+}	0.00	0.16 (7)	−0.05 (2)	0.03 (3)	−0.06 (2)	−0.09 (4)	0.02 (2)
P_{11-}	0.00	0.00	0.05 (2)	0.10 (3)	0.00	0.00	0.00
P_{20}	0.08 (4)	−0.42 (5)	−0.14 (2)	−0.19 (2)	−0.14 (2)	−0.31 (4)	−0.25 (2)
P_{22-}	0.00	0.20 (5)	−0.01 (2)	−0.01 (2)	−0.06 (2)	−0.01 (3)	0.02 (3)
P_{22+}	0.00	0.00	0.10 (2)	−0.08 (2)	0.00	0.00	0.00
P_{31+}	0.00	0.03 (4)	0.00 (2)	−0.04 (3)	−0.03 (2)	−0.04 (5)	0.03 (2)
P_{31-}	0.00	0.00	−0.02 (2)	−0.02 (3)	0.00	0.00	0.00
P_{33+}	0.00	0.40 (6)	0.20 (2)	0.24 (3)	0.13 (3)	0.48 (4)	−0.38 (2)
P_{33-}	0.00	0.00	0.01 (2)	0.12 (3)	0.00	0.00	0.00
P_{40}	−0.40 (4)	0.15 (4)	−0.04 (2)	−0.01 (3)	−0.03 (3)	0.08 (6)	−0.02 (2)
P_{42+}	0.00	0.06 (4)	0.05 (2)	0.04 (3)	0.04 (3)	0.02 (6)	−0.01 (2)
P_{42-}	0.00	0.00	−0.01 (3)	0.02 (3)	0.00	0.00	0.00
P_{44+}	−0.26 (4)	0.26 (5)	0.03 (3)	0.00 (3)	0.02 (3)	−0.02 (5)	0.02 (2)
P_{44-}	0.00	0.00	0.02 (2)	0.03 (3)	0.00	0.00	0.00

	H(2)	H(7)		H(2)	H(7)
κ	1.04 (5)	1.14 (5)	P_V	1.10 (10)	0.79 (6)
$\kappa'\zeta$	2.33 (21)	1.91 (18)	P_{10}	0.30 (3)	0.27 (3)

[a] ζ in au^{-1}, populations in *e*. [b] Values without standard deviations were not refined. [c] Symmetry constraints: C(3) = C(2), C(4) = C(1), C(11) = C(10) = C(9) = C(8) = C(7), H(3) = H(2), H(11) = H(10) = H(9) = H(8) = H(7).

refinement (refinement II). The scale factor was obtained by one cycle of refinement of k with all other parameters fixed.

Since the crystal structure of CoTPP is acentric, experimental deformation densities suffer from the fact that only the amplitude and not the phase of the structure factor $\vec{F}_0$ can be determined from the experiment.[19] If the phases of the $\Delta\vec{F}$ are distributed at random, then the result will generally be a reduction in the size of features in the deformation density by a factor between 0.5 and 1.0.[24]

When a fit to the density has been obtained by a multipole deformation refinement, a *model* deformation density may be calculated

$$\Delta\rho_{\text{model}} = \rho_{\text{model}} - \sum\rho_{\text{spherical atoms}}$$

Since the phases of the model structure factors are known, these maps do not suffer the same phase uncertainty problem as the observed deformation maps. In addition, the limited flexibility of the model acts as a filter for noise introduced in maps as a result of errors in the experimental observations. It is, of course, necessary to check that the model has not failed to fit significant features of the experimental density. This is easily done by plotting the residual density

$$\Delta\rho_{\text{residual}} = \rho_{\text{obsd}}/k - \rho_{\text{model}}$$

The significance of features in the observed or residual densities can be judged by comparison with a plot of the distribution of estimated standard deviation of $\Delta\rho$. Errors in the experimental observations contribute an approximately uniform uncertainty of 0.04 e/Å^3 (not including the uncertainty in the phase), while errors in the positional and thermal parameters and X-ray scale factor yield a contribution which peaks sharply at the atomic centers. Plots of the error distribution, $\sigma(\Delta\rho)$, have been calculated as described previously and include an approximate correction for series termination effects.[25,26]

Results and Discussion

Refinement Results. Despite the lower accuracy of the weak high-order reflections, the R factors and "goodness of fit" parameters are better for the refinement of only high-order data (refinement II) than for the refinement of the full data set (refinement I). This is, of course, due to the fact that the conventional spherical atom model used in X-ray analysis is more appropriate for the high-order reflections where the scattering is primarily from the more nearly spherical core electron distributions. The estimated standard deviations of the high-order parameters, however, are significantly higher.

The R factors are also much lower for the multipole deformation refinement (refinement III), indicating that a significant fraction of the disagreement between observed and calculated structure factors in the conventional refinement may be attributed to deficiencies in the spherical atom model for the valence electron distribution.

Interatomic distances and angles calculated from the conventional, high-order, and multipole deformation refinement parameters (uncorrected for thermal motion) are compared in Table V along with the corresponding values determined at room temperature.[10] Estimated standard deviations in distances and angles are calculated by using the full least-squares variance–covariance matrix.

As expected, the effect of the aspherical electron distribution on the conventional refinement results is largest for the hydrogen positions. The resulting C–H bond distances are 0.1–0.2 Å shorter than typical internuclear separations as determined by neutron diffraction. The fact that the C–H distances in the high-order and multipole refinements differ from the value of 1.09 Å set at the start of refinement reflects the relaxation of the carbon atom position during refinement.

Comparison of the conventional results with either the high-angle or multipole refinement results indicates that, except for hydrogen, the asphericity shifts are quite small. This is likely a result of both the presence of high-order data in the conventional refinement and the generally symmetrical arrangement of valence density features around each atom other than hydrogen.

An exception, however, is observed for the nitrogen atom which according to the high-order refinement shifted by 0.010 (3) Å relative to the conventional refinement position in a direction approximately perpendicular to the Co–N bond. The anomalous nitrogen position is probably due to errors in the high-order data since there is no chemical explanation for such an asphericity shift. Also, the multipole refinement result is in closer agreement with the conventional refinement nitrogen position. Another exception is C10 which is shifted in the high-order refinement by 0.013 (7) Å in the general direction of H10.

Another way of assessing the reliability of the refinement results is to compare the bond distances and angles of chemically equivalent but crystallographically independent bonds. Although crystal-packing effects may have some influence, particularly for torsion angles of the phenyl groups, the effects on bond distances are expected to be insignificant. Comparison of equivalent distances in Table V reveals surprisingly that the agreement between equivalent bonds for the high-order refinement is slightly worse than for the conventional refinement, although the anomalous position of the nitrogen atom certainly is responsible for much of the disagreement. On the other hand, the agreement between

(24) Savariault, J.-M.; Lehmann, M. S. *J. Am. Chem. Soc.* **1980**, *102* 1298–1303.
(25) Rees, B. *Acta Crystallogr, Sect. A* **1976**, *A32*, 483–488.
(26) Stevens, E. D.; Coppens, P. *Acta Crystallogr., Sect. A* **1976**, *A32*, 915–917.

Table V. Bond Distances (Å) and Angles (Deg)

	refinement			room temp[a]
	I	II	III	
	Bond Distances			
Co–N	1.949 (1)	1.953 (2)	1.949 (1)	1.949 (3)
N–C1	1.379 (2)	1.381 (3)	1.378 (1)	1.387 (4)
N–C4	1.380 (2)	1.366 (3)	1.377 (1)	1.378 (4)
C1–C2	1.433 (2)	1.439 (4)	1.442 (1)	1.426 (5)
C3–C4	1.442 (2)	1.442 (3)	1.440 (1)	1.443 (5)
C2–C3	1.354 (2)	1.352 (5)	1.362 (1)	1.346 (5)
C4–C5	1.386 (2)	1.385 (4)	1.392 (1)	1.384 (5)
C1–C5′	1.394 (2)	1.395 (4)	1.390 (1)	1.396 (5)
C5–C6	1.488 (2)	1.486 (3)	1.488 (1)	
C6–C8	1.395 (2)	1.400 (5)	1.393 (1)	
C6–C10	1.389 (2)	1.396 (4)	1.394 (1)	
C8–C9	1.387 (2)	1.388 (4)	1.391 (2)	
C10–C11	1.390 (2)	1.391 (5)	1.393 (1)	
C9–C7	1.388 (2)	1.394 (6)	1.389 (2)	
C11–C7	1.388 (2)	1.389 (7)	1.387 (1)	
C2–H2	0.90 (3)	1.089	1.085	
C3–H3	0.89 (3)	1.093	1.086	
C7–H7	0.90 (2)	1.084	1.087	
C8–H8	0.97 (3)	1.088	1.090	
C9–H9	0.90 (2)	1.087	1.088	
C10–H10	0.98 (3)	1.080	1.086	
C11–H11	0.95 (3)	1.092	1.091	
	Bond Angles			
N–Co–N	90.01 (2)	90.01 (2)	90.01 (2)	90.00 (2)
Co–N–C1	127.7 (1)	127.0 (1)	127.4 (1)	127.5 (2)
Co–N–C4	127.1 (1)	127.3 (2)	127.4 (1)	127.4 (2)
N–C1–C2	110.7 (1)	110.2 (2)	110.7 (1)	110.4 (3)
N–C4–C3	110.4 (1)	110.5 (2)	110.9 (1)	110.3 (3)
C1–C2–C3	107.0 (1)	106.8 (2)	106.7 (1)	107.5 (3)
C4–C3–C2	106.8 (1)	106.9 (2)	106.6 (1)	106.8 (3)
C1–N–C4	105.1 (1)	105.6 (2)	105.1 (1)	105.0 (3)
C2–C1–C5′	124.2 (2)	124.2 (2)	123.7 (1)	124.6 (3)
C3–C4–C5	123.3 (1)	122.9 (2)	123.1 (1)	123.4 (3)
C4–C5–C6	118.7 (1)	119.2 (2)	118.5 (1)	119.0 (3)
C1′–C5–C6	119.1 (1)	119.1 (2)	119.6 (1)	118.0 (3)
C8–C6–C10	118.8 (1)	119.0 (2)	118.9 (1)	
C6–C10–C11	120.9 (1)	120.2 (3)	120.5 (1)	
C6–C8–C9	120.6 (1)	120.6 (3)	120.7 (1)	
C10–C11–C7	119.8 (1)	120.6 (4)	120.1 (1)	
C8–C9–C7	120.0 (1)	120.2 (4)	120.0 (1)	
C9–C7–C11	119.9 (1)	119.4 (3)	119.8 (1)	

[a] From ref 10.

equivalent bonds for the multipole refinement is excellent; always being within the estimated standard deviation of the difference.

Deformation Density Maps. The observed deformation density calcuated in the plane of the pyrrole ring is shown in Figure 1. As observed in numerous previous studies on smaller molecules, peaks are found in the deformation density between all covalently bounded atoms and in the lone pair region of the nitrogen atom. In addition, sharp peaks are located at only 0.4 Å from the cobalt site in directions bisecting the N–Co–N angles. The latter are clearly a result of the preferential occupancy of the d orbitals in the low-spin electron configuration.

The estimated distribution of errors in the deformation density in the plane of the pyrrole ring is plotted in Figure 2. Except near the atomic centers, where the uncertainty increases rapidly to over 0.7 e Å^{-3}, the estimated $\sigma(\Delta\rho)$ is 0.04 e Å^{-3}. Inspection of the peaks in the deformation density of chemically equivalent bonds reveals differences which are generally within 3–4 times the estimated $\sigma(\Delta\rho)$. In other areas not near atomic sites or bonding regions, the noise level is consistent with the estimated $\sigma(\Delta\rho)$.

The noise level in the deformation density can be reduced by averaging the observed density over chemically equivalent regions of the molecule.[25,27] The observed deformation density in the plane of the pyrole ring after averaging the left and right sides together is plotted in Figure 3. Even after averaging, however, features of the observed deformation density are poorly resolved in comparison with recent low-temperature, high-resolution studies of small molecules.[28] Several of the bond peaks run togehter and

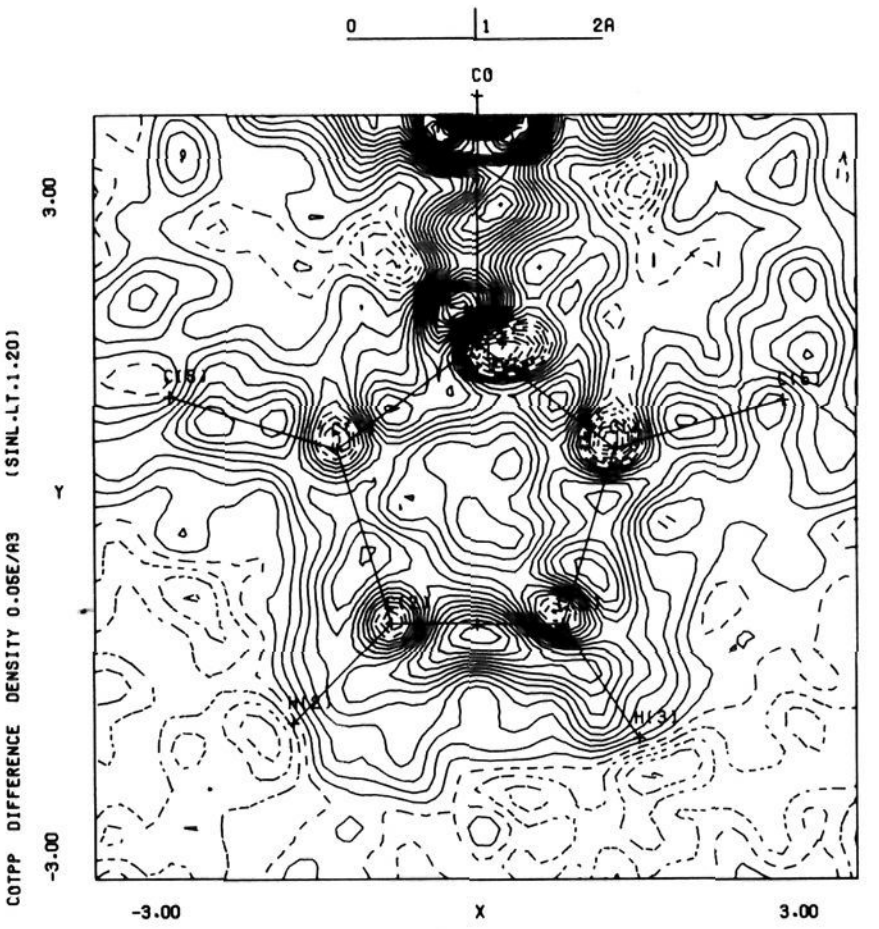

Figure 2. Observed deformation density plotted in the plane of the pyrrole ring. Contours are at 0.05 e Å^{-3} intervals with zero and negative contours dashed.

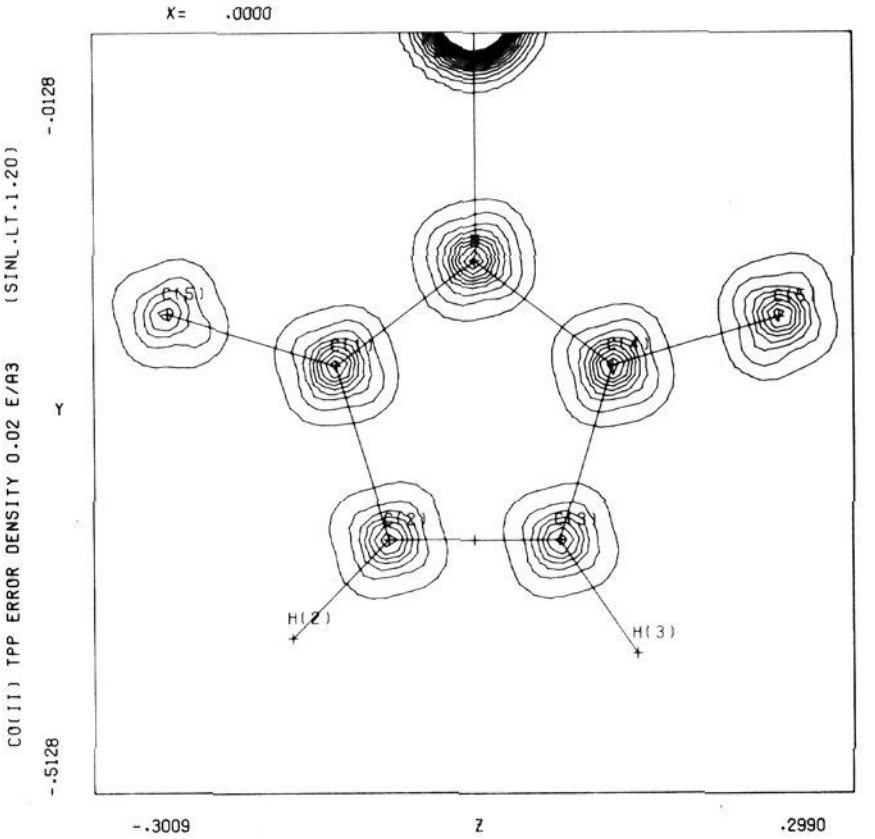

Figure 3. Contour plot of the distribution of the estimated standard deviation in the observed deformation density calculated for the same plane as in Figure 2. Contours are at 0.02 e Å^{-3} intervals, lowest contour plotted at 0.04 e Å^{-3}.

(27) Bénard, M.; Coppens, P.; DeLucia, M. L.; Stevens, E. D. *Inorg. Chem.* **1980**, *19*, 1924–1930.

(28) See, for example: Stevens, E. D.; Coppens, P. *Acta Crystallogr. Sect. B* **1980**, *B36*, 1864–1876. Stevens, E. D. *Ibid.* **1978**, *B34*, 544–551.

(29) Iwata, M.; Saito, Y. *Acta Crystallogr., Sect. B* **1973**, *B29*, 822–832. Marumo, F.; Isobe, M.; Saito, Y.; Yagi, T.; Akimoto, S. *Ibid.* **1974**, *B30*, 1904–1906. Ohba, S.; Toriumi, K.; Sato, S.; Saito, Y. *Ibid.* **1978**, *B34*, 3535–3542.

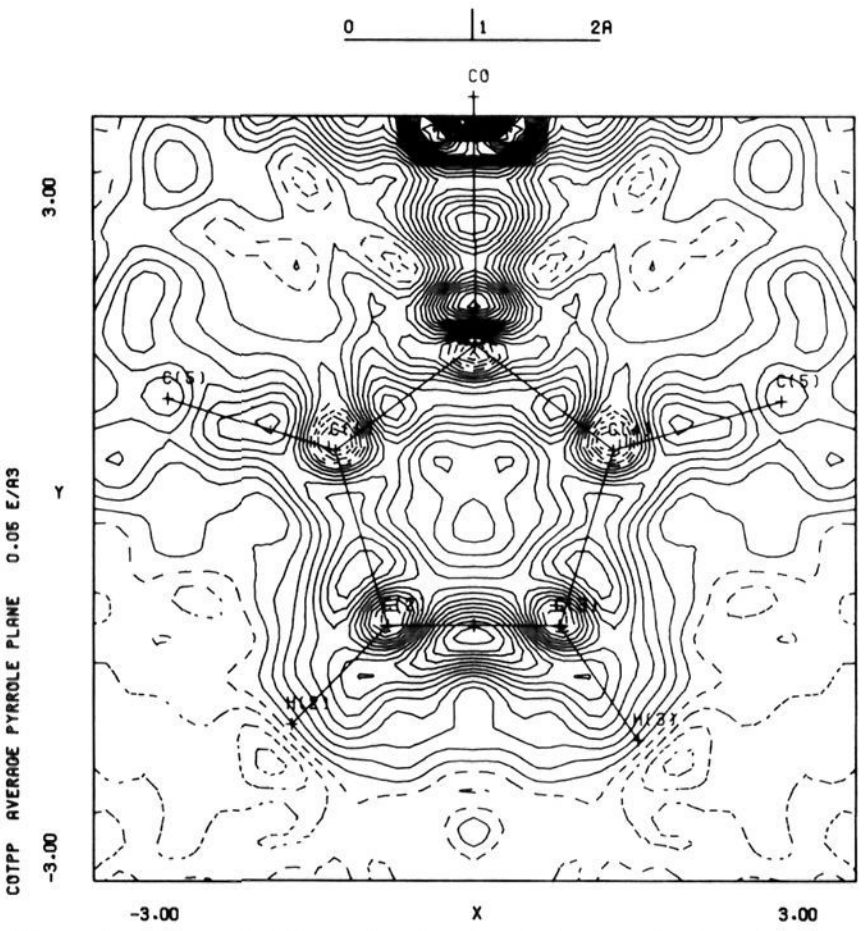

Figure 4. Observed deformation density in the pyrrole ring after left–right averaging about the Co–N bond direction. Contours are as in Figure 2.

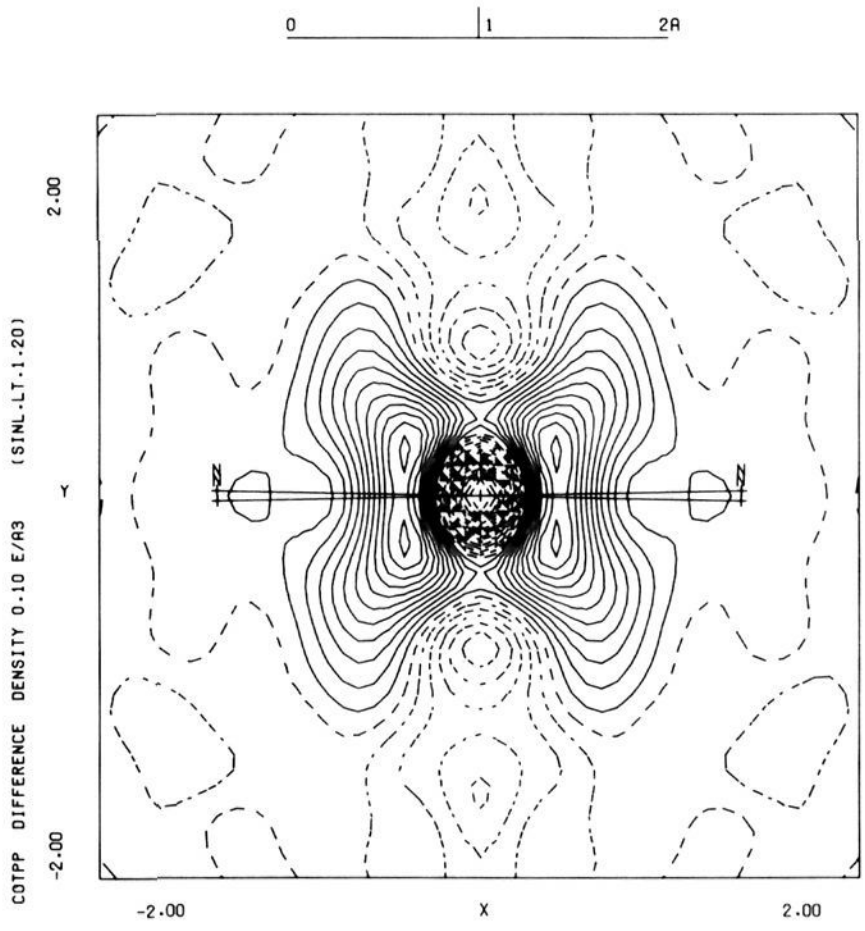

Figure 6. Observed deformation density plotted in a plane perpendicular to the porphyrin ring and bisecting the N–Co–N angle. Contours are as in Figure 5.

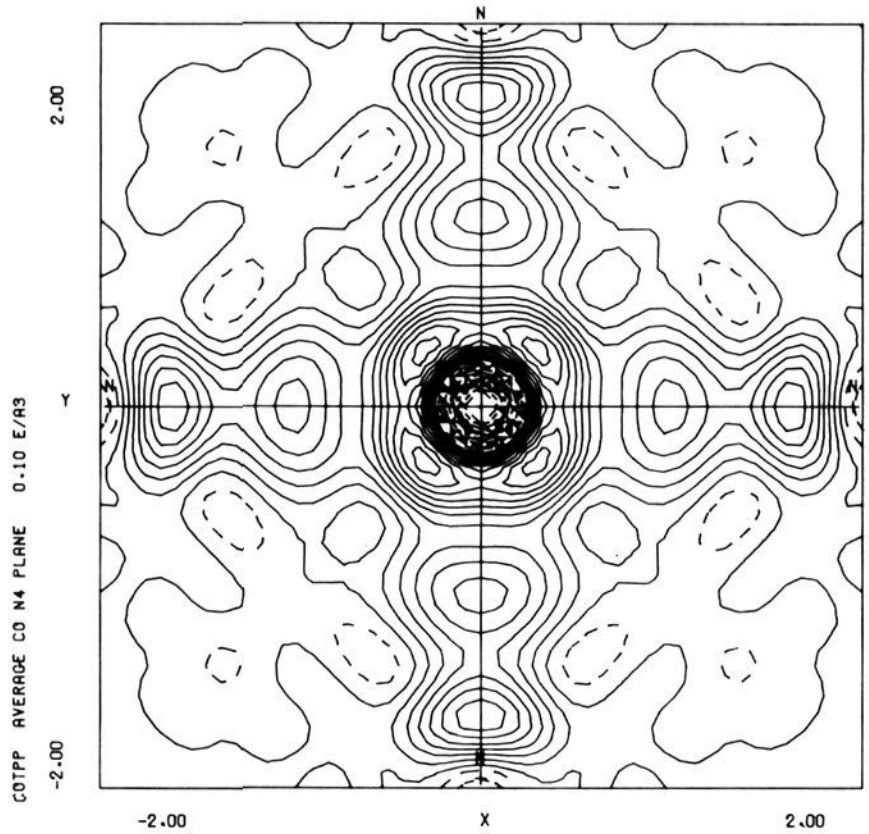

Figure 5. Observed deformation density plotted in the plane of the porphyrin ring, centered at the cobalt site. The density has been left–right averaged. Contours are at 0.10 eÅ^{-3} intervals with zero and negative contours dashed.

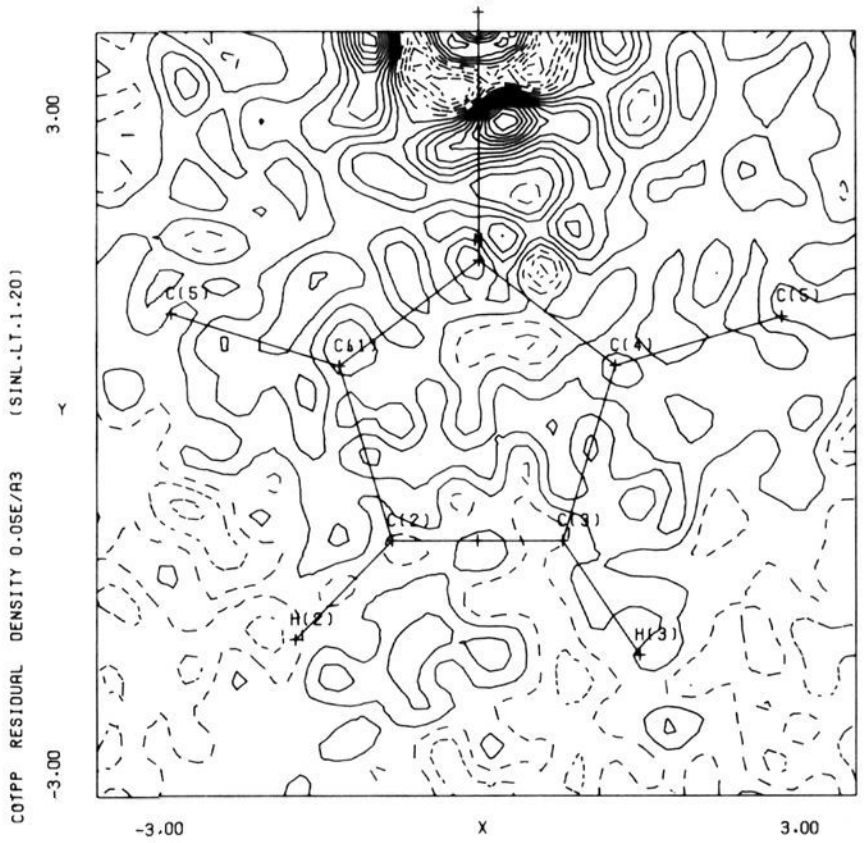

Figure 7. Residual density from the multipole refinement plotted in the pyrrole plane. Contours are as in Figure 2.

the nitrogen lone pair and C1–C2 bond peaks show double maxima. Much of this lack of definition in the observed density may be attributed to the uncertainty in the phases of the observed structure factors.[19,24]

The observed density at the Co site in the porphyrin plane (also averaged) is plotted in Figure 5. The four peaks which appear surrounding the metal atom in the porphyrin plane are not true maxima in the deformation density. A plot of the deformation density in a plane perpendicular to the molecular plane and bisecting the N–Co–N angle (Figure 6) shows that the true maxima lie above and below the molecular plane pointing into the faces of a coordination octahedron defined by the four nitrogen atoms and the two unoccupied axial sites. This electron distribution is remarkably similar to those which have been found for low-spin octrahedrally coordinated metal complexes.[5,6,27] The peaks indicate a maximum deformation of 1.1 (1) e Å^{-3} relative to an isolated (high-spin) cobalt atom, located 0.45 Å from the atomic center. The actual magnitude of the d-electron deformation will, of course, vary depending on the amount of smearing due to thrmal motion in the crystal and the resolution of the X-ray experiment.

A small, generally negative deformation is observed near the metal atom in the axial directions. This is consistent with the ESR studies of four-coordinated cobalt porphyrins which indicate the single unpaired electron occupies the d_{z^2} orbital.[30]

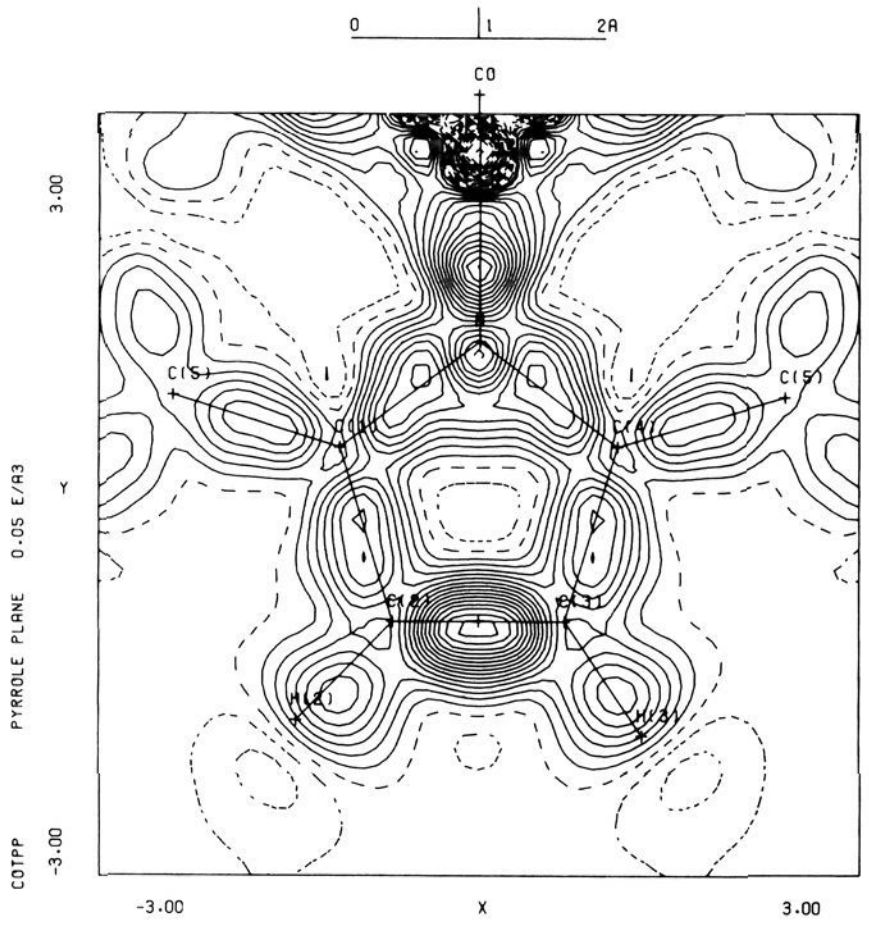

Figure 8. Model deformation density plotted in the plane of the pyrrole ring. Contours are as in Figure 2.

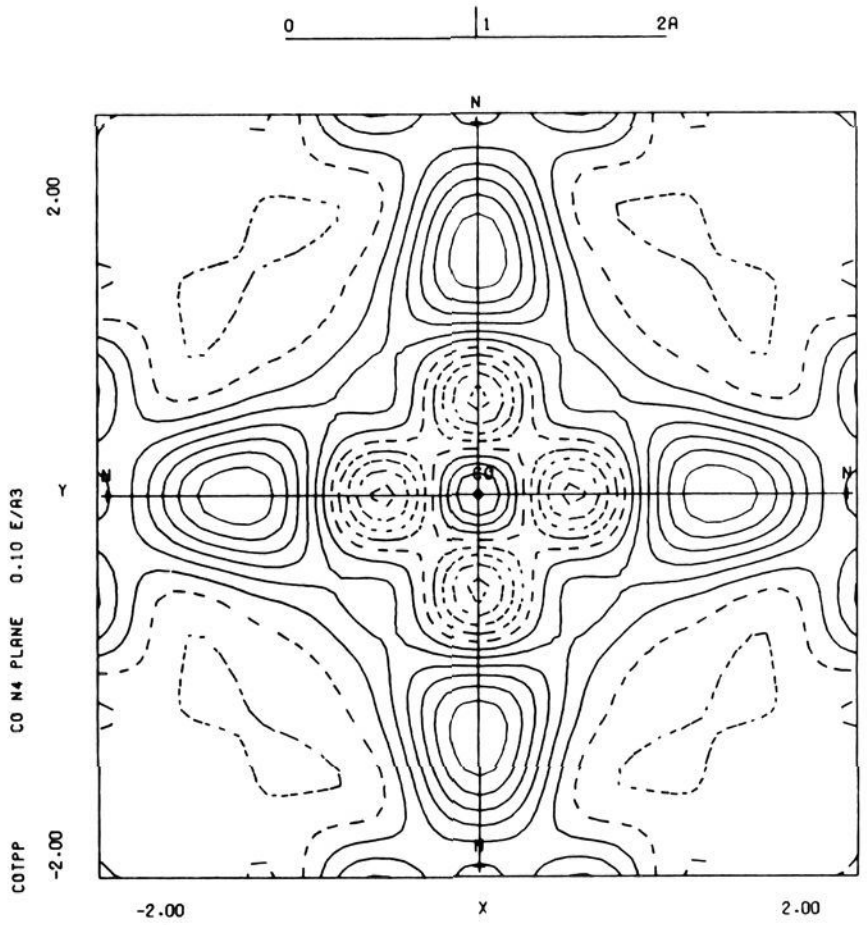

Figure 9. Model deformation density plotted in the plane of the porphyrin ring, centered at the cobalt site. Contours are as in Figure 5.

A plot of the residual density from the multipole refinement in the plane of the pyrrole ring (Figure 7) demonstrates a good fit of the model in the region of the porphyrin molecule. Features of the residual are generally within $2-3\sigma(\Delta\rho)$. A similar fit is obtained in the region of the phenyl groups. The fit is significantly worse, however, closer to the metal atom. A peak of 0.56 e $Å^{-3}$ remains in the residual density between the cobalt and nitrogen atoms. Since the multipole deformation functions of the cobalt atom must accommodate the sharper features of the d-electron distribution, the model apparently lacks sufficient flexibility to fit this peak. It should also be noted that errors due to improper phase estimates and systematic effects such as errors in the correction for absorption will tend to be largest near the metal atom site.

The model deformation density in the pyrrole plane is shown in Figure 8. Noncrystallographic symmetry has been imposed on the pyrrole ring by constraining the multipole populations of chemically equivalent atoms to be equal. Compared to the observed deformation maps, the model deformation density shows smoother, more distinct features and the lack of experimental noise. The peaks are also somewhat higher as expected from the improved phase treatment.[24] Only a single peak is now observed in the nitrogen lone-pair region, although a very slight double maxima remains in the C1–C2 bond peak.

The model density near the cobalt atom in the plane of the porphyrin molecule (Figure 9) shows a more negative deformation along the Co–N bond close to the cobalt site. Such a negative deformation is expected for a low-spin electron configuration which yields a formally unoccupied $d_{x^2-y^2}$ orbital. Positive deformation peaks are again observed near Co above and below the porphyrin plane (Figure 10).

Both observed and model deformation maps yield a peak in the C2–C3 bond which is substantially larger than other covalent bond peaks in the porphyrin or phenyl rings. A section of the model density perpendicualr to the C2–C3 bond and passing through the bond midpoint (Figure 11) shows a significant deviation of the bond peak from cylindrical symmetry in the direction perpendicular to the ring. The deviation of the bond density from cylindrical symmetry becomes more apparent if the difference is

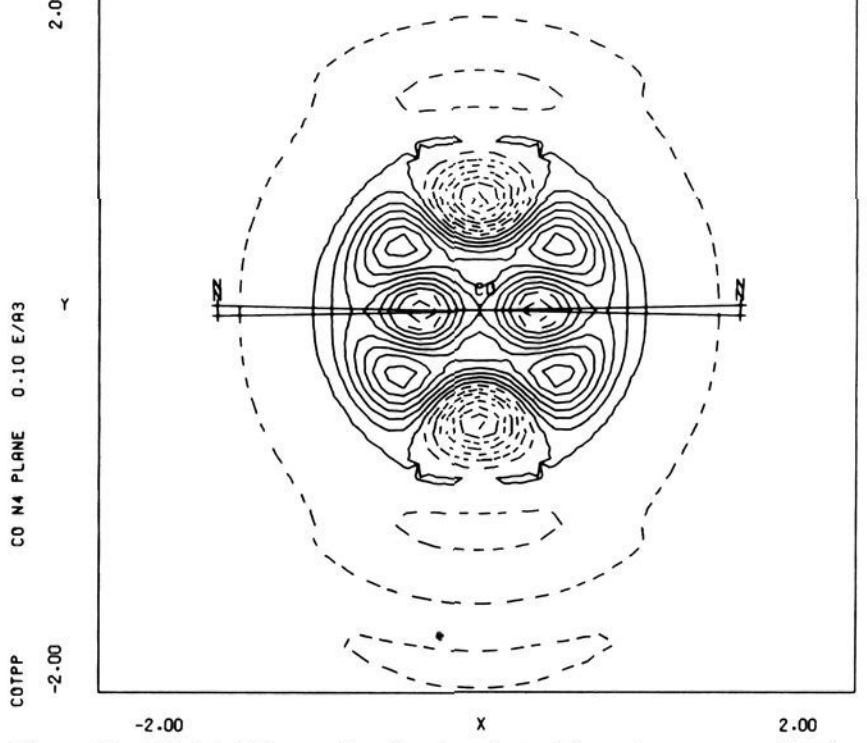

Figure 10. Model deformation density plotted in a plane perpendicular to the porphyrin ring and bisecting the N–Co–N angle. Contours are as in Figure 5.

calculated between Figure 11 and the same figure rotated by 90° about the bond axis.[4] This double difference density

$$\Delta(\Delta\rho) = \Delta\rho - \Delta\rho(90°)$$

is plotted for the C2–C3 bond in Figure 12. Similar maps have been calculated for other peaks in the CoTPP deformation density, and the maximum deviations from cylindrical symmetry are listed in Table VI. The larger deviation observed in the C2–C3 bond as compared with other bonds in the porphyrin molecule can be explained in terms of a greater degree of localization of the π bonding in the C2–C3 bond. This is in agreement with proposed resonance structures for the porphyrin ring which include isolated double bonds at the C2–C3 position to satisfy the $4n + 2$ rule for aromaticity.[31]

(30) Lin, W. C. *Inorg. Chem.* **1976**, *15*, 1114–1118. Lin W. C. In "The Porphyrins"; Dophin, D., Ed.; Academic Press: New York, 1979; Vol. IV, pp 355–377.

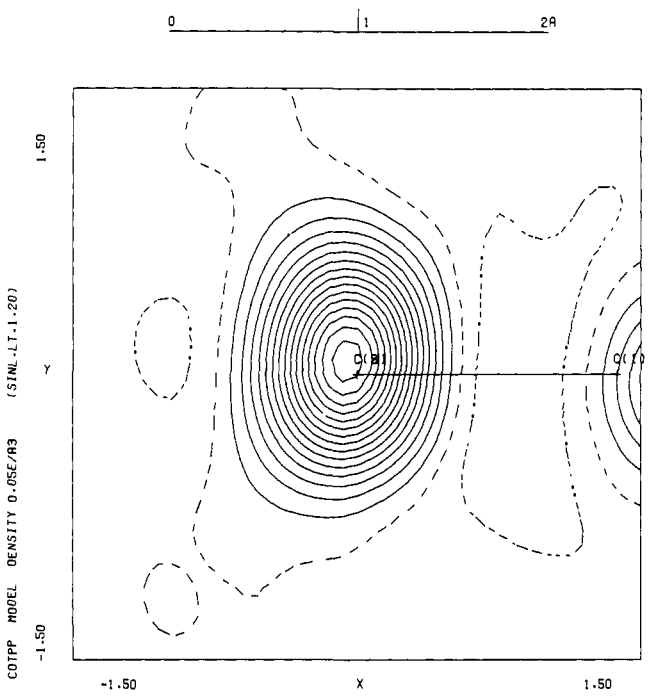

Figure 11. Model deformation density plotted in a plane perpendicular to and bisecting the C2–C3 bond. Contours are as in Figure 2. The orientation of the pyrrole ring is indicated by the projection of the C1–C2 bond onto the plane.

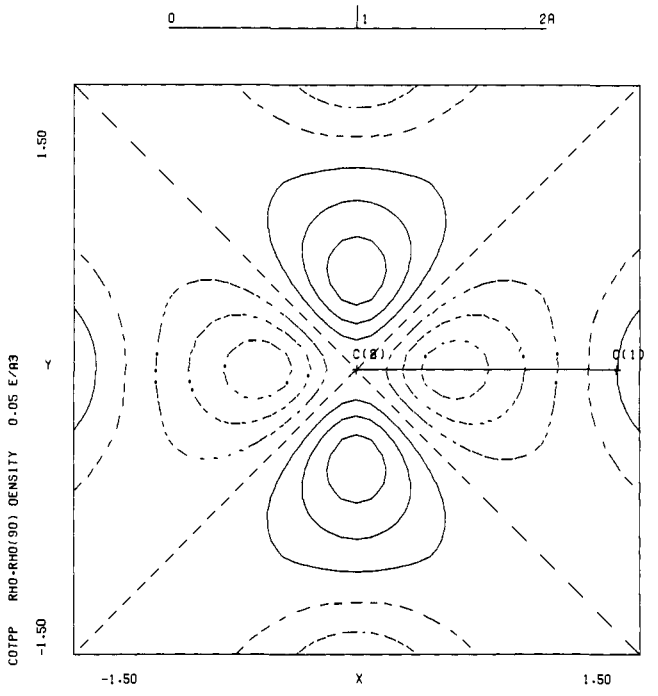

Figure 12. Plot of the deviation of the C2–C3 bond peak from cylindrical symmetry. Contours as in Figure 2. The orientation of the pyrrole ring is indicated by the projection of the C1–C2 bond onto the plane.

Table VI. Maximum Deviations of Deformation Bond Peaks from Cylindrical Symmetry (in e Å^{-3})[a]

bond	obsd density	model density
Co–N	0.03	0.08
N–C1	0.08	0.06
C1–C2	0.12	0.15
C2–C3	0.22	0.18
C4–C5	0.18	0.14
C5–C6	−0.05	0.09
C6–C8	0.11	0.10

[a] Estimated standard deviation in all values is 0.04 e Å^{-3}.

The extent to which the improved phase estimates are responsible for the difference in appearance between the observed and model deformation densities can be investigated by a calculation using the observed structure factors with phases from the multipole model refinement. A deformation density map calculated in such a manner (including left-right averaging) is shown in Figure 13. When Figure 13 is compared with Figures 4 and 8, it is apparent that much of the difference between the observed and model densities near the cobalt atom, in the nitrogen lone pair, and in the shapes of the bond peaks can be attributed to the difference in the treatment of the phases.

d-Orbital Populations. Consider, as a first approximation, that the atomic wave function of the metal can be described by a single Slater determinant and that the d-electron wave function may be described by a minimal set of orbitals consisting of the products of Slater-type radial functions and the usual spherical harmonic angular functions. With the further assumption, in the cyrstal field approximation, that covalent interactions between the metal atom and the ligands may be ignored, then the electron density distribution corresponding to the 3d electrons may be expressed simply in the form where P_1, P_2, P_3, and P_4 are orbital occupancies

$$\rho_{3d} = P_1(d_{x^2-y^2})^2 + P_2(d_{z^2})^2 + P_3(d_{xy})^2 + P_4(d_{xz}^2 + d_{yz}^2)$$

and the d_{xz} and d_{yz} orbitals remain degenerate in a tetragonally octahedral field.

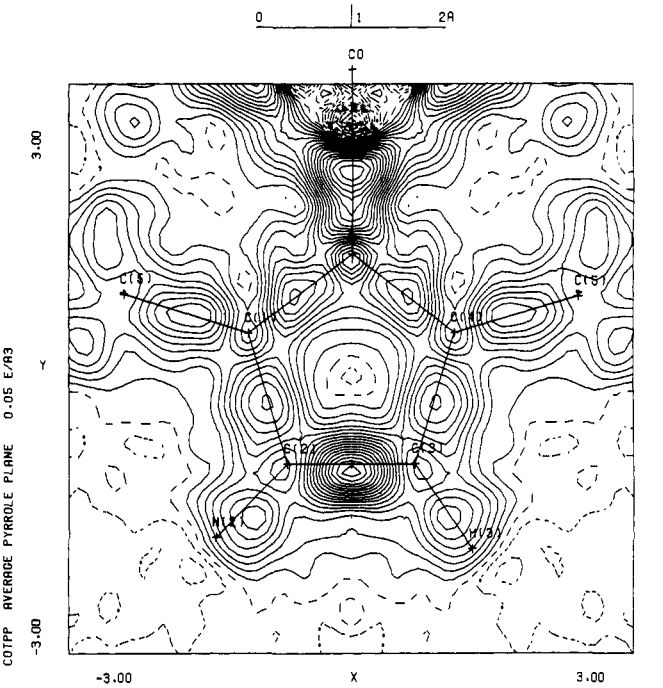

Figure 13. Plot of the observed deformation density in the plane of the pyrrole ring calculated by using phases from the model deformation refinement. Contours are as in Figure 2.

The squares of the angular functions of the 3d orbitals may be expressed as a sum of spherical harmonic functions of order 0, 2, and 4. These angular functions are the same as the symmetry-allowed density functions included in the multipolar deformation refinement of the X-ray data. The following linear relationship can be shown between the d-orbital occupancies and the multipolar density function populations, P_{lm}[32]

$$P_{00} = (1/4\pi)^{1/2}C_{00}(P_1 + P_2 + P_3 + P_4)$$

(31) Codding, P. W.; Tulinsky, A. *J. Am. Chem. Soc.* **1972**, *94*, 4151–4157.

(32) Stevens, E. D. In "Electron and Magnetization Densities in Molecules and Crystals"; Becker, P., Ed.; Plenum Press: New York, 1980; pp 823–826. Stevens, E. D.; Coppens, P. *Acta Crystallogr., Sect. A* **1979**, *A35*, 536–539.

$$P_{20} = (5/196\pi)^{1/2}C_{20}(-2P_1 + 2P_2 - 2P_3 + P_4)$$

$$P_{40} = (1/196\pi)^{1/2}C_{40}(P_1 + 6P_2 + P_3 - 4P_4)$$

$$P_{44+} = (5/28\pi)^{1/2}C_{44}(-P_1 + P_3)$$

where $C_{lm} = N_{lm}$(wave function)$/N_{lm}$(density function), since the density functions are not normalized in the same manner as the wave functions. These equations are easily solved to yield the d-orbital occupancies from the X-ray multipole populations.

The d-orbital occupancies obtained from refinement III are given in Table VII along with the expected populations for high- and low-spin Co(II). The total number of d electrons has been constrained to seven during refinements. The estimated standard deviations of the populations include the effect of correlation between the least-squares parameters. The occupancies obtained from the X-ray data differ significantly from the populations expected for an isolated (high-spin) cobalt atom and are generally in closer agreement with a low-spin configuration. The refined radial parameter is also quite reasonable for cobalt 3d electrons. The value of $\zeta = 3.80$ (2) au^{-1} corresponds to a slightly expanded d shell compared with the optimized Slater exponent of 3.95 au^{-1} calculated for an isolated neutral cobalt atom[33]

The observed d-orbital populations provide a description of the electronic structure at the metal atom which is limited by the initial assumptions. Some of the populations differ from integer values, and the population of the $d_{x^2-y^2}$ orbital is much higher and the population of the d_{xy} orbital is lower than expected for a low-spin configuration. One of the assumptions made was that the atomic wave function could be descried in the form of a single Slater determinant. A limited calculation by Lin[30] indicates that several additional electron configurations may contribute to the ground state. Apparent orbital populations have been calculated including the mixing of excited configurations as obtained by Lin and are included in Table VII. These populations deviate from the ideal low-spin occupancies in the same direction as the experiment, although not to the same extent.

Another initial assumption was that covalent bonding between metal and ligand atoms could be ignored. A covalent contribution to the bonding between cobalt and the porphyrin molecule may be expected to affect the apparent orbital occupancies. For example, σ donation from the ligand to metal would increase the $d_{x^2-y^2}$ population, while π back-donation would decrease the populations of the d_{xz} and d_{yz} orbitals.

Conclusions

The feasibility of obtaining information on the electronic structure of metalloporphyrins from accurate X-ray diffraction measurements of the electron density distribution has been demonstrated. High-resolution measurements of CoTPP at low temperature yield an experimental charge distribution with an accuracy comparable to those currently obtained for small molecule structures. A large deformation in the C2–C3 bond elongated perpendicular to the molecular plane indicates considerable localized double-bond character.

A fit to the X-ray data using a multipole refinement model yields improved estimated for the structure factor phases. The influence of the phase uncertainty on the experimental electron distribution is sufficiently large to make such a treatment of the phases mandatory for future studies of acentric metalloporphyrins. In addition, the refined multipole populations on the metal atom can be used to derive approximate-d-electron configurations. The derived d-orbital occupancies show some deviation from the expected low-spin electron configuration, which may be attributed to the effects of mixing of excited configurations and covalency in the metal–ligand bonding. The accuracy of such studies on metalloporphyrins appears equal to similar studies on smaller inorganic and organometallic systems.

The experimental electron distribution of CoTPP may now be used to calculate other physical properties. Of particular interest for iron porphyrins will be calculation of the electric field gradient at the iron nucleus which may be compared with Mossbäuer quadrupole splitting measurements.[5] The experimental electron distribution of CoTPP also provides a sensitive three dimensional property against which various theoretical models may be tested.

Table VII. CoTPP d-Orbital Occupancies

	expected			
atomic orbital	high spin	low spin	obsd	calcd[a]
P_1 $b_1(d_{x^2-y^2})$	1.4	0.0	1.0 (2)	0.25
P_2 $a_1(d_{z^2})$	1.4	1.0	1.0 (2)	1.06
P_3 $b_2(d_{xy})$	1.4	2.0	1.3 (2)	1.76
P_4 $e(d_{xz},d_{yz})$	2.8	4.0	3.7 (3)	3.91

[a] Apparent occupancies including mixing of excited configurations as calculated by Lin.[30]

Acknowledgment. The author wishes to thank Professor P. Coppens for his active encouragement of this project and Miss D. L. Chadwick for assistance in preparation of the figures. Support of this work by the National Institutes of Health (Grant HL-23884) is gratefully acknowledged.

Supplementary Material Available: A listing of the final observed and calculated structure amplitudes (14 pages). Ordering information is given on any current masthead page.

(33) Clementi, E.; Raimondi, D. L. *J. Chem. Phys.* **1963**, *38*, 2686–2689.